2011 50th IEEE Conference on Decision and Control and
European Control Conference (CDC-ECC)
Orlando, FL, USA, December 12-15, 2011

Gabor filter and eigen-flame image-based burning state recognition for sintering process of rotary kiln

Weitao Li, Kezhi Mao, Tianyou Chai, Hong Zhang, and Hong Wang

Abstract— **Accurate recognition of burning state is critical in sintering process control of rotary kiln. Recently, flame image-based burning state recognition has received much attention. However, most of the existing methods demand accurate image segmentation, which is quite challenging due to poor image quality caused by smoke and dust inside the kiln. In this study, we develop a more reliable method for burning state recognition without image segmentation issue. From the experience of operators, more discriminable flame and material zones will facilitate the subsequent feature extraction and burning state recognition. Motivated by this knowledge, we propose to include texture analysis based on Gabor filter as a pre-processing to improve the recognition result further and then extract global features based on eigen-flame images decomposition, and finally recognize the burning state using pattern classifier. The advantages of our method are threefold. Firstly, our Gabor filter selection approach can generate a compact filter bank to distinguish ROIs much more and offers help to facilitate the sequel. Secondly, the eigen-flame image method provides global features of an image with large class separability and hence can lead to more accurate classification performance. Thirdly, the new method is more robust and reliable than image segmentation-based methods and temperature-based method. Experimental studies show the effectiveness of our method.**

I. INTRODUCTION

Rotary kiln is widely used in metallurgical, cement, chemical and environment protection industries. The main control objective of sintering process of rotary kiln is to achieve consistent product quality, which are often referred to as key performance indexes. However, practically, the measurement of the product quality index is done by manual sampling with one-hour period. Therefore, online control is impossible to be realized and indirect control is employed, i.e. keeping measurable key process parameters and are closely related to the product quality index into their preset ranges means satisfied product quality index. Based on the analysis of rotary kiln mechanism process, the fact that burning zone temperature directly determines the characteristics of the clinker is widely acknowledged. Thus, most of the current control strategies for rotary kiln take this temperature as the controlled variable [1], [2], [3]. The accurate measurement for such temperature is hence the most critical issue for the rotary kiln sintering process. However, due to the harsh environment inside the kiln, the accurate measurement for such temperature through thermocouple is challenging.

For operators, burning zone flame image with rich and reliable visual information is considered to be more reliable than the burning zone temperature to estimate the burning state. In this study, a flame image-based burning state recognition method is employed, with the goal of improving the burning state recognition result. Previously, flame image-based burning state recognition has been studied already, and is mostly based on image segmentation techniques [4], [5], [6]. However, since the smoke and dust disturbance in the kiln, flame images are often with poor quality, and accurate segmentation of region of interests (ROIs) is still a challenging task. This will in turn result in inaccurate feature extraction and poor state recognition result.

The configuration of ROIs, i.e. the flame zone and the material zone, is the key factor to recognize the burning state for operation experts. In the present study, global configuration feature of flame image will be extracted to recognize the burning state to avoid the difficult image segmentation. Before feature extraction, according to operators' experience, more discriminable ROIs will facilitate the subsequent feature extraction and burning state recognition. Motivated by the knowledge that ROIs are with distinct texture characteristics, we employ texture analysis in a pre-processing step to facilitate the sequel. Owing to its optimal localization in both spatial and frequency domains, Gabor filter has emerged as one of the most popular approaches to texture analysis [7]. Practically, its parameter is often set by trial and error. Although a large Gabor filter bank produces high-dimensional feature representation with large discriminative power, it is not expected from the perspective of pattern classification due to the peaking phenomenon [8]. In the present study, we propose to incorporate Mahalanobis separability measure and forward feature selection technique [8] to filter bank design to automatically generate a compact filter bank, which not only saves computational cost but also enhances the discrimination of ROIs to facilitate the sequel. Such Gabor filter selection method has been successfully applied to standard texture image analysis [9], but not on flame image before.

After the pre-processing by Gabor filter, eigen-flame images are then obtained using principal component analysis (PCA), and the global features of flame images are finally

This work was supported by National Basic Research Program of China2009CB320601), the Plan for University Subject Innovation and Introducing Intelligence (B08015), and Natural Science Foundation of China (61020106003)

W.T. Li and T.Y. Chai are with the State Key Laboratory of Synthetical Automation for Process Industries, Northeastern University, Shenyang, 110004, China lwt1981@yahoo.cn

K.Z. Mao is with with the School of Electrical and Electronic Engineering, Nanyang Technological University, Singapore, 639798, Singapore

H. Zhang is with Department of Computing Science, University of Alberta, Edmonton, T6G-2P8, Canada

H. Wang is with Key Laboratory of Synthetical Automation for Process Industries (Northeastern University), Shenyang, 110819, China. He is also with the Control System Center, University of Manchester, Manchester, M601QD, United Kingdom.

produced by correlating each flame image with the eigen-flame images, and are used as input to probabilistic neural network pattern classifier (PNN) [12] to obtain the burning state recognition result. Eigen-image decomposition has been successfully applied to some image recognition applications [10], [11], but it has never been used in the flame image burning state recognition before. Unlike traditional selection criterion for eigen images from a low-dimensional reconstruction viewpoint [10], [11], a new eigen-flame image selection procedure based on Fisher ratio measure is employed in our work, with the goal of selecting global features that possess the maximum discriminative power to enhance the recognition performance for flame images. This eigen-flame image method has been used to flame image burning state recognition, but without the Gabor filter pre-processing step [13]. Here, the incorporation of the pre-processing step is expected to improve the recognition result further. The advantages of our burning state recognition method are threefold. Firstly, our Gabor filter selection approach can generate a compact filter bank to distinguish ROIs much more and offers help to facilitate the sequel. Secondly, the eigen-flame image method provides global features of an image with large class separability and hence can lead to more accurate classification performance. Thirdly, the new method is more robust and reliable than image segmentation-based methods and temperature-based method. Experimental studies show the effectiveness of our method.

The rest of the paper is organized as follows. The rotary kiln sintering process and hybrid control strategy is presented in Section 2. In Section 3 gives our new burning state recognition method based on flame image. Experimental studies and conclusions and future work are given in Section 4 and 5 respectively.

II. Description of rotary kiln sintering process and hybrid control strategy

A schematic diagram of rotary kiln sintering process consisting of feeding system, burning system and smoke exhausting system is shown in Fig. 1 [14].

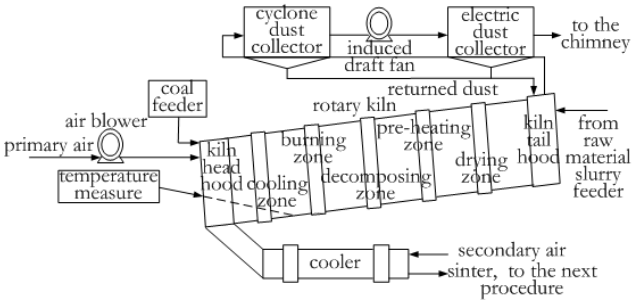

Fig. 1. Schematic diagram of rotary kiln sintering process

• Feeding system: From the kiln tail, raw material slurry is sprayed into the kiln for heat exchange with the heated gas from coal powders. After residing 50∼70 min within the kiln, produced clinker drops into the cooler and then is fed downstream for further processing.

• Burning system: Coal powders from the coal feeder and primary air from the air blower are mixed into a bi-phase fuel flow, sprayed into the kiln head hood, and then combust with secondary air from the cooler. The heated gas is brought to the kiln tail by the induced draft fan.

• Smoke exhausting system: Via cyclone dust collector, dust particle of the exhaust gas is fed into the kiln through pipeline. The purified exhausting gas is brought to the electric dust collector for further purification, and then is discharged into the air.

Recently, we have successfully developed and implemented a hybrid control system consisting of a burning state recognizer, a coal feeding level estimator, a supervisory MIMO fuzzy controller, and a human mimic controller for No. 3 rotary kiln at Shanxi Aluminum Corp as shown in Fig. 2 [15]. In such hybrid control system, the burning state recognizer is based on clustering of temperatures from the non-contact colormetric measuring device and control strategies switch accordingly. The function of each module is briefly described as follows.

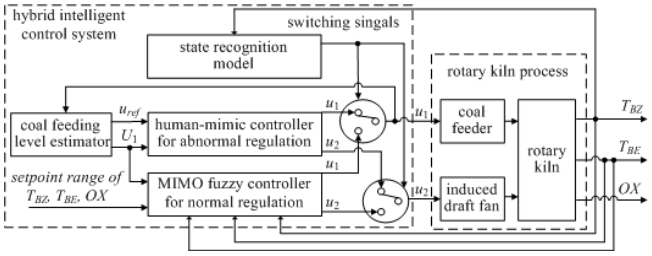

Fig. 2. Structure of control system for rotary kiln sintering process

A. Coal feeding level estimator

Due to the special large lag, the kiln heat supply, i.e. the coal feeding u_1, should be kept relatively smooth with relatively smooth boundary conditions to maintain the stable distribution of the kiln temperature. In our study, U_1, namely the current coal feeding level, is introduced to characterize u_1 and defined by

$$U_1 = (u_{1_{avg}} - u_{ref})/u_{ref} \tag{1}$$

where $u_{1_{avg}}$ and u_{ref} denote the most recent moving average value of u_1 and coal feeding reference value over a preset time interval respectively.

B. Supervisory MIMO fuzzy controller for normal phase

During the normal phase, based on the opening and closing and intelligent decoupling strategies, the supervisory MIMO fuzzy controller is to coordinate the coal feeding u_1 and the damper position of the induced draft fan u_2 so that burning state temperature T_{BZ}, kiln tail temperature T_{BE} and residual oxygen contents in combustion gas OX satisfy the technical requirements. Currently, with the restricted state of the damper position of the induced draft fan $IDBC$ and OX, four different rule-bases are used for different

conditions. Each rule in each rule-base is defined as:

$$\textbf{IF } e^i_{T_{BZ}} \textit{ and } \triangle T^j_{BZ} \textit{ and } e^l_{T_{BE}} \textit{ and } U^k_1 \textbf{ then } \triangle u^m_1 \textit{ and } \triangle u^n_2 \quad (2)$$

where i, j, l, k, m and n denote the indices of fuzzy sets. $e_{T_{BZ}}$ and $e_{T_{BE}}$ are the error signal between the current T_{BZ} and T_{BE} and their setpoints. $\triangle u_1$ and $\triangle u_2$ are the corrections of u_1 and u_2. For each rule-base, the number of rules for $\triangle u_1$ part is 135, plus another 135 for the $\triangle u_2$ part, giving a total of 270 rules.

C. Human mimic controller for abnormal phase

In abnormal phase, due to the special large lag, the effect of the instant coal feeding will be postponed. Such case will lead to large periodic oscillation of T_{BZ}. The human mimic controller based on gain scheduling is to avoid the overshoot when large disturbance happens.

Based on U_1 and u_{ref}, the acceptable total correction for the coal feeding u_{total} is defined as $u_{total} = K_1 K_2 u_{ref}$, where K_2 is defined by

$$K_2 = min(max(1 + K_3 U_{1_{SW}}, 1 + K_3), 1 - K_3) \quad (3)$$

where $U_{1_{SW}}$ in Eq(3) means U_1 at the controller switching time t_{SW}, and K_1 and K_3 are constants. For each control period, the output of the controller is determined by

$$\triangle u_1(t) = \begin{cases} K u_{total} & \textit{if } \sum_{t_i} \triangle u_1(t_i) \le u_{total} \\ & (t_i = t, t-1, \ldots, t_{SW}) \\ 0 & \textit{else} \end{cases} \quad (4)$$

where K is a gain coefficient. u_2 remains constant to avoid influencing combustion condition during the abnormal phase.

III. Robust recognition of burning zone state based on flame image

A. Problems on burning zone temperature measurement

Based on the analysis of rotary kiln mechanism process, T_{BZ} directly determines the characteristic of clinker, and both higher and lower T_{BZ} will deteriorate the quality of clinker [14]. Via the measurement of T_{BZ}, burning state is recognized and control strategies are switched accordingly. Hence, the accurate measurement of T_{BZ} is considered as the most critical issue for the sintering process of rotary kiln.

Previously, thermocouples are inserted through the kiln shell along the kiln to measure T_{BZ}. However, these are considered unreliable by operators, since fouling occurs on the thermocouples located in the most interesting region, i.e. burning zone. In our hybrid control system, T_{BZ} is measured through the non-contact colormetric measuring device and burning state is assessed according to the clustering of T_{BZ}. Unfortunately, due to the disturbance from dust and smoke and the limitation of the temperature measurement device itself, such a single point temperature measurement is often far from its true value and often exhibits great fluctuation and severe noise. Hence, the unreliable measurement often results in inferior burning state recognition result and inconsistent product quality. The accurate measurement of T_{BZ} is still a challenging task.

To alleviate the problems involved in the temperature measurement and imitate the burning state estimation of experienced human operators, an intelligent burning state recognizer based on burning zone flame image for the above hybrid control system is studied in the present study, with the goal of replacing the existing recognizer to achieve more reliable and accurate burning state recognition.

B. Burning zone flame image

As shown in Fig. 3, a flame image consists of a few parts including kiln wall, coal zone, material zone and flame zone, where the configuration of the flame zone and material zone are the key factors in burning state recognition.

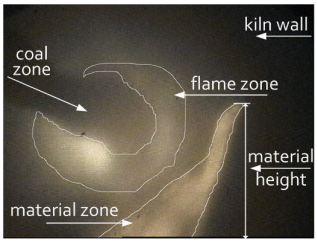

Fig. 3. A burning zone flame image

Previously, before adopting features to represent the above key factors, ROIs are firstly obtained by image segmentation techniques. However our studies found, due to the turbulent flame bouncing around and the harsh environment inside the kiln, difficult tracking of the accurate boundary of ROIs for flame images with poor quality will in turn lead to inaccurate feature extraction and poor burning state recognition result.

To avoid the problems confronted in image segmentation methods, we have tried to extract features of flame image to recognize burning state without the difficult step of segmentation which have not been applied before. Procedure of our method is described as follows.

C. Pre-processing of flame image

Based on our analysis, distinct texture characteristics is for the flame zone and material zone. This knowledge motivates the application of texture analysis to distinguish such two zones as the pre-processing step to facilitate the subsequent global feature extraction and burning state recognition.

Gabor filter [16], [17], [18], as a joint entropy minimizing frequency sensitive filter, is employed as the pre-processing step to distinguish such zones. Practically, parameters of Gabor filter are often set by trial and error. However, we believe only a subset of the filters might be useful, while others are either redundant or insignificant and offer little improvement to (or even reduce) the discriminative power due to the peaking phenomenon. In our study, a new approach is developed to generate a compact filter bank, which not only save computational cost for texture representations and remove potential bias by "trial and error" designing pattern, but also enhance the discrimination of ROIs much more to facilitate the sequel.

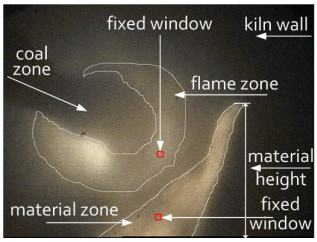

Fig. 4. Fixed windows of flame image

Due to the camera placement providing a rough estimate for the trajectory and range for material and flame zones respectively, we will use two 25×25 fixed windows to sample the flame zone and material zone respectively as shown in Fig. 4 to avoid the difficulty of the segmentation issue. Assume a total of $2P$ material and flame texture images from P training flame images: $\boldsymbol{T}_1, \boldsymbol{T}_2, \ldots, \boldsymbol{T}_{2P}$. Let $\boldsymbol{z}_1, \boldsymbol{z}_2, \ldots, \boldsymbol{z}_{n_G}$ denote feature groups extracted from filtered texture images by the n_G initial constructed filters, where $\boldsymbol{z}_k = [z_{1,k}, z_{2,k}, \ldots, z_{2P,k}]^T$. For each texture image, the mean μ and the standard deviation σ features are extracted, i.e. $z_{i,k} = [\mu_{i,k}, \sigma_{i,k}]$. Mahalanobis separability is employed as the metric function to evaluate and sort the discriminative power of feature groups $\boldsymbol{z}_k$ and associated Gabor filters, and is defined as follows:

$$J_k = (\boldsymbol{m}_{i,k} - \boldsymbol{m}_{j,k})\boldsymbol{C}_k^{-1}(\boldsymbol{m}_{i,k} - \boldsymbol{m}_{j,k})^T \qquad (5)$$

where $\boldsymbol{m}_{i,k}$, $\boldsymbol{m}_{j,k}$ and $\boldsymbol{C}_k$ denote mean vector and covariance matrix of material class and flame class in feature space along feature group $\boldsymbol{z}_k$ respectively. In our study, this metric is combined with a forward feature selection technique to automatically select uncorrelated feature groups and associated Gabor filters to best distinguish material and flame zones of training flame images. The proposed filter selection approach is briefly illustrated as follows:

(i) For each $\boldsymbol{z}_k$, calculate J_k using (5). Assume $J_{k_1} \geq J_{k_2} \geq \ldots \geq J_{k_{n_G}}$. $\boldsymbol{z}_{s_1}$ with J_{k_1} is selected as the first candidate feature subset, denoted as $\boldsymbol{f}_1 = \{\boldsymbol{z}_{s_1}\}$.

(ii) Each of the remaining feature groups is combined with $\boldsymbol{f}_1$ to form $n_G - 1$ subsets $\boldsymbol{f}_2 = \{\boldsymbol{z}_{s_1}, \boldsymbol{z}_j\}(j \in 1, \ldots, n_G, j \neq s_1)$. Calculate Mahalanobis measure for the $n_G - 1$ subsets using (5). Subset $\{\boldsymbol{z}_{s_1}, \boldsymbol{z}_{s_2}\}(s_2 \in 1, \ldots, n_G, s_2 \neq s_1)$ with the maximum measure is selected as the second candidate feature subset, denoted as $\boldsymbol{f}_2 = \{\boldsymbol{z}_{s_1}, \boldsymbol{z}_{s_2}\}$.

(iii) Perform classification on each of the n_G candidate feature subsets $\{\boldsymbol{z}_{s_1}\}, \{\boldsymbol{z}_{s_1}, \boldsymbol{z}_{s_2}\}, \ldots, \{\boldsymbol{z}_{s_1}, \boldsymbol{z}_{s_2}, \ldots, \boldsymbol{z}_{s_{n_G}}\}$. The filter bank corresponding to the n_s^{th} subset with the best performance is regarded as the final optimal compact Gabor filter bank.

Please refer to [9] for details.

D. Eigen-flame image decomposition and global feature extraction

Once the optimal compact bank with n_s Gabor filters for training dataset is selected, for each training flame image $\boldsymbol{F}$, the mean image $\boldsymbol{F}'$ of n_s filtered images is used to substitute $\boldsymbol{F}$ to form a new training image. To avoid the problems associated with image segmentation, in our study, we will use eigen-flame image decomposition based on PCA for global feature extraction of flame image.

Assume $\boldsymbol{F}'_1, \boldsymbol{F}'_2, \ldots, \boldsymbol{F}'_P$ represent P new generated training flame images. $\boldsymbol{Y}_1, \boldsymbol{Y}_2, \ldots, \boldsymbol{Y}_P$ are eigen-flame images after applying PCA to the training dataset. Due to the correlation coefficients between a flame image and the eigen-flame images can be considered as global feature to represent the flame image, the selection for the eigen-flame images is hence quite important. Unlike traditional selection criterion that is optimal from a low dimensional reconstruction viewpoint, Fisher ratio [19] is employed as the metric function to select eigen-flame images possessing large class separability which has not been applied to flame image before. The class separability I_l of the l^{th} eigen-flame image $\boldsymbol{Y}_l$ is defined as:

$$I_l = \frac{\sum_{i=1}^{N_C}\sum_{j=1}^{N_C}\frac{|g_{i,p}-g_{j,p}|^2}{s_{i,p}^2+s_{j,p}^2}}{N_C(N_C-1)} \ (l = 1, \ldots, P) \qquad (6)$$

where $g_{i,l}$, $g_{j,l}$, $s_{i,l}$, $s_{j,l}$, and N_C denote mean and standard deviation of flame image class C_i and class C_j correlated with $\boldsymbol{Y}_l$ and the image class number respectively.

Once the I_l of all $\boldsymbol{Y}_l$ are evaluated, the eigen-flame images selection, i.e. extraction of optimal global features, can be carried on. Followed by the same procedure, a testing flame image is firstly filtered by the designed compact Gabor filter bank, and then the global features are extracted by correlating the filtered image with the selected eigen-flame images, and the features are finally sent to PNN classifier trained to obtain the recognition result. See [13] for its details.

IV. Experiments

In order to validate the proposed method, flame images of the burning zone under various conditions are collected from No. 3 rotary kiln. A color CCD camera and a non-contact colorimetric temperature measure device are installed outside the peephole of the kiln head. The output signal of CCD is digitized using an image grabber card. Each RGB digital image has a size of 512×384 pixels. The sampling period for flame image and burning zone temperature is set to 10 seconds.

A total of 482 typical flame images, including 86 over-burning, 193 under-burning and 203 normal-burning images are selected to form a image database, based on which bootstrapping [20] with 2000 replica is performed to estimate the accuracy of flame image burning state recognition. Some examples are shown in Fig. 5. The labeling of these images is done by rotary kiln operational experts.

As described in Section III.C, Fig. 6 shows the classification result of training material and flame data versus candidate Gabor filter bank used during one sampling experiment. As shown in Fig. 6, optimal recognition result is achieved on the training data when the eight most discriminative Gabor filters are used. Thus, such a compact filter bank was selected for training and testing flame images throughout

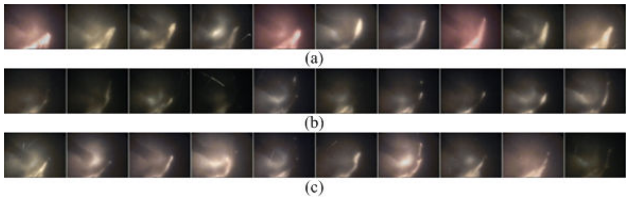

Fig. 5. Some typical flame images: (a) over-burning (b) under-burning (c) normal-burning

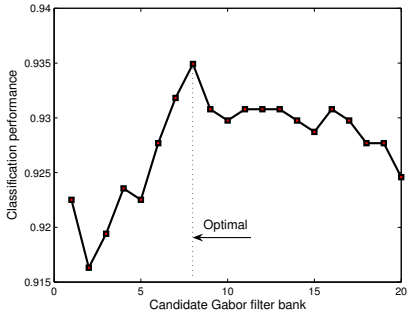

Fig. 6. Classification performance vs. Candidate Gabor filter bank

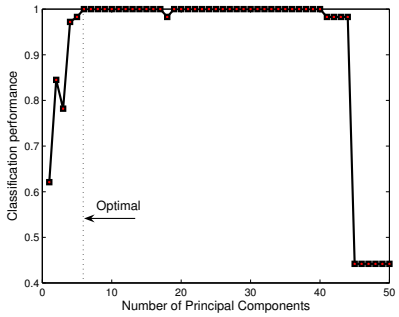

Fig. 7. Correct recognition rate vs. Number of eigen-flame images

TABLE I
COMPARISON OF RECOGNITION RESULTS

Eigen-Flame Image Method	Color Space	Accuracy(%) (With Filter)	Accuracy(%) (Without Filter)
With selection of eigen-flame Images	HSV	89.72±5.4	84.67±6.2
	RGB	86.57±5.7	81.89±6.8
	YIQ	85.63±5.6	80.78±6.1
	Gray	86.78±6.0	81.42±6.4
Without selection of eigen-flame images	HSV	84.25±5.9	76.45±6.7
	RGB	80.42±6.2	75.23±6.6
	YIQ	80.53±6.5	73.79±6.5
	Gray	81.76±5.9	74.68±7.2

this sampling experiment. It is worth noting that, peaking phenomenon occurs in the Gabor filter bank design procedure, i.e. high-dimensional feature representation leading to a gradual degradation classification performance. Hence, Gabor filter bank design is not a subjective parameter designing and filter bank creating procedure, but filter selection should be an indispensable part for such procedure.

Once the eight optimal Gabor filters are obtained, Fig. 7 shows the state recognition accuracy versus the candidate eigen-flame image combinations used, i.e. the number of global features or principal components. In Fig. 7, 100% correct recognition is achieved on the training data when the six most discriminative eigen-flame images are used. Thus, such six eigen-flame images are selected for testing flame images throughout this sampling experiment.

Flame images captured by the CCD camera are RGB images. In this study, we have explored the performance of our algorithm in other color spaces including HSV, YIQ and gray scale. Moreover, in order to validate the effectiveness of Gabor filter for the state recognition, we have also tested the performance of our algorithm without the Gabor filter procedure. Again, considering the labeling of kiln operational expert as ground truth, the classification accuracy is presented in the format of mean±standard deviation of 2000 repeats as listed in Table 1.

From Table 1, we have the following observations:

a) The best result is achieved in HSV space and there is little difference between the other three spaces. This is probably because the HSV space is a non-linear transformation of RGB, while the transformations of RGB to YIQ and gray scale are linear. HSV is more compatible to human perception pattern.

b) By selecting the eigen-flame images, the global features obtained substantially outperform those without selection. This is because PCA is optimal from a low-dimensional reconstruction viewpoint and is non-optimal from the pattern classification point of view.

c) Independently of color space and eigen-flame image selection methods, Gabor filter pre-processing enhances the discrimination of the flame and material zones and offers help to the subsequent global feature extraction and burning state recognition.

Further, the effectiveness of our filter bank selection procedure and the impact of various classifiers for the burning state recognition are also studied. The performance of our eigen-flame image-based algorithm combined with various filter bank design methods and our burning state recognition algorithm combined with various classifiers are shown in Table 2 and Table 3 respectively. As shown in Table 2, our filter bank design approach not only selects the uncorrelated filters and leads to a more compact filter bank, but also distinguishes the flame and material zones much more to facilitate the sequel. PNN is essentially based on the well-known Bayesian classification technique, and considers the probability characteristic of sample space. Therefore, although the number of principal components and Gabor filters are not minimum both, the classification performance has the best result in Table 3.

We also compared our method with temperature-based burning state recognition. Taking the labeling of kiln operational experts as ground truth, the recognition accuracy of the two methods at the same time is 89.72% and 81.34% at the same time. Again, our method outperforms the temperature-

TABLE II

COMPARISON OF RECOGNITION RESULTS

Filter Design Methods	Average Accuracy (%)	No. of Gabor filters
Our method-based	89.72±5.4	8.1±3.7
Fisher ratio-based	88.12±5.2	10.0±4.1
D.A. Clausi et al.[16]	86.94±6.3	24
S. Li et al.[15]	86.78±5.8	36
F. Bianconi et al.[17]	87.58±5.9	288

TABLE III

COMPARISON RESULTS FOR VARIOUS CLASSIFIER METHODS

	PNN	NN	SVM
Average accuracy (%)	89.72±5.4	88.22±2.4	86.38±1.7
No. of PCs	7.9±2.3	12.5±2.1	5.8±1.0
No. of Gabor filters	8.1±3.7	8.5±3.3	9.2±4.3

based method and is more reliable even with the disturbance of dust and smoke inside the kiln.

Finally, we compared our method with four image segmentation-based methods including Ostu, FCM and Gabor wavelet (FCMG) [5], Dual fast marching (DFM) [6] and multistage adaptive threshold (MAT) [21]. Also, all studies are in HSV color space. Based on the experience of kiln operational experts, the following features of ROIs are extracted in segmentation based methods: average brightness of V sub-image, average brightness and its variance of the flame and material zones of V sub-image, area, length, width, circularity, and barycentric coordinates of the flame zone, and height, width, area, and barycentric coordinates of the material zone. All these features are then sent to PNN pattern classifier to obtain the recognition result. The average classification accuracy of 2000 repeats with different classifiers is shown in Table 4. Again, in our study, regardless of various segmentation methods, PNN gives the best result. Moreover, in our application, due to the images with poor quality leading to inaccurate ROIs segmentation and feature extraction, the above segmentation-based methods are substantially inferior to our method and could work well only when the flame images are of high quality.

V. CONCLUSIONS AND FUTURE WORK

In this study, we have explored the feasibility of applying Gabor filter to distinguish ROIs as a pre-processing step to improve the recognition result further and using eigen-flame image decomposition for flame image global feature extraction and burning state recognition. Experimental studies have demonstrated the effectiveness of our proposed approach. It is expected that improved product quality index could be achieved if the new method is incorporated into our previously hybrid control system. Implementation of this new method in our system is the next work.

TABLE IV

RECOGNITION RESULTS FOR DIFFERENT SEGMENTATION METHODS

Methods	PNN	NN	SVM
Ostu-based	42.67±11.4	40.26±11.1	41.79±11.2
FCMG-based	44.72±12.3	41.62±12.5	42.83±12.1
DFM-based	47.23±11.5	44.31±12.3	46.32±13.2
MAT-based	52.19±11.3	49.29±12.3	51.78±11.3

REFERENCES

[1] C.W. Ruby, "A new approach to expert kiln control", *in XXXIX IEEE Conference on Cement Industry Technical*, Hershey, PA, 1997, pp 339-412.

[2] M. Akalp, A.L. Dominguez and R. Longchamp, "Supervisory fuzzy control of a rotary cement kiln", *in 7th IEEE Conference on Electrotechnical*, Mediterranean, 1994, pp 754-757.

[3] M. Jarvensivu, K. Saari and S.L. Jamsa-Jounela, Intelligent Control System of an Industrial Lime Kiln Process, *Control Engineering Practice*, vol. 9, 2001, pp 589-606.

[4] S.T. Li and Y.N. Wang, Segmentation of kiln flame image based on neural networks, *Chinese Journal of Scientific Instrument*, vol. 22, 2001, pp 10-14.

[5] P. Sun, T.Y. Chai and X.J. Zhou, "Rotary Kiln Flame Image Segmentation Based on FCM and Gabor Wavelet Based Texture Coarseness", *in 7th World Congress on Intelligent Control and Automation*, Chongqing, China, 2008, pp 7615-7620.

[6] H.Y. Jiang, X.L. Cui, X.J. Zhou and T.Y. Chai, Image segmentation based on improved dual fast marching method, *Journal of System Simulation*, vol. 3, 2008, pp 803-810.

[7] M. Idrissa and M. Acheroy, Texture classification using Gabor filters, *Pattern Recognition Letters*, vol. 23, 2002, pp 1095-1102.

[8] A.K. Jain, R.P.W. Duin and J.C. Mao, Statistical Pattern Recognition: A Review, *PAMI*, vol. 22, 2000, pp 4-37.

[9] W.T. Li, K.Z. Mao, H. Zhang and T.Y. Chai, "Designing Compact Gabor Filter Banks for Efficient Texture Feature Extraction", *in International Conference on Control, Automation, Robotics and Vision*, Singapore, Singapore, 2010, pp 1193-1198.

[10] J. Yang, D. Zhang, A.F. Frangi and J.Y. Yang, Two-dimensional PCA: a new approach to appearance-based face representation and recognition, *IEEE Transactions on Pattern Analysis and Machine Intelligence*, vol. 26, 2004, pp 131-137.

[11] M. Turk and A. Pentland, Eigenfaces for recognition, *Journal of Cognitive Neuroscience*, vol. 3, 1991, pp 71-86.

[12] D.F. Specht, Probabilistic neural network, *Neural Network*, vol. 3, 1990, pp 109-118.

[13] W.T. Li, K.Z. Mao, X.J. Zhou, T.Y. Chai and H. Zhang, "Eigen-flame image-based robust recognition of burning states for sintering process control of rotary kiln", *in IEEE Conference on Decision and Control*, Shanghai, China, 2009, pp 398-403.

[14] Z.Y. Yang, *Alumina production technology*, Metallurgical industry press, Beijing; 1982.

[15] X.J. Zhou and T.Y. Chai, "Pattern-based Hybrid Intelligent Control for Rotary Kiln Process", *in IEEE International Conference on Control Applications*, Singapore, 2007, pp 31-35.

[16] S. Li and J.S. Taylor, Comparison and fusion of multiresolution features for texture classification, *Pattern Recognition Letters*, vol. 26, 2004, pp 633-638.

[17] D.A. Clausi and H. Deng, Design-based texture feature fusion using Gabor filters and co-occurrence probabilities, *IEEE Trans. Image Process*, vol. 14, 2005, pp 925-936.

[18] F. Bianconi and A. Fernández, Designing compact Gabor filter banks for efficient texture feature extraction, *Pattern Recognition*, vol. 40, 2007, pp 3325-3335.

[19] R.O. Duda and P.E. Hart, *Pattern Classification and Scene Analysis*, Wiley, New York; 1973.

[20] M.R. Chemick, *Bootstrap methods: A practitioner's guide*, Wiley, New York; 1999.

[21] F.X. Yan, H. Zhang and C.R. Kube, A multistage adaptive thresholding method, *Pattern Recognition Letters*, vol. 26, 2005, pp 1183-1191.